GEOPHYSICS, VOL. 82, NO. 2 (MARCH-APRIL 2017); P. Q1–Q12, 16 FIGS.
10.1190/GEO2016-0162.1

Elastic internal multiple analysis and attenuation using Marchenko and interferometric methods

Carlos Alberto da Costa Filho[1], Giovanni Angelo Meles[1], and Andrew Curtis[1]

ABSTRACT

Conventional seismic processing aims to create data that contain only primary reflections, whereas real seismic recordings also contain multiples. As such, it is desirable to predict, identify, and attenuate multiples in seismic data. This task is more difficult in elastic (solid) media because mode conversions create families of internal multiples not present in the acoustic case. We have developed a method to predict prestack internal multiples in general elastic media based on the Marchenko method and convolutional interferometry. It can be used to identify multiples directly in prestack data or migrated sections, as well as to attenuate internal multiples by adaptively subtracting them from the original data set. We developed the method on two synthetic data sets, the first composed of horizontal density layers and constant velocities, and the second containing horizontal and vertical density and velocity variations. The full-elastic method is computationally expensive and ideally uses data components that are not usually recorded. We therefore tested an acoustic approximation to the method on the synthetic elastic data from the second model and find that although the spatial resolution of the resulting image is reduced by this approximation, it provides images with relatively fewer artifacts. We conclude that in most cases where cost is a factor and we are willing to sacrifice some resolution, it may be sufficient to apply the acoustic version of this demultiple method.

INTRODUCTION

The presence of multiples (i.e., waves that have reflected multiple times) causes errors in many fields, such as nondestructive testing (Taheri and Honarvar, 2016), medical imaging (Feldman et al., 2009), and exploration seismology within methods such as migration, reflection tomography, and velocity estimation (Yilmaz, 2001). Although a variety of different methods exist to predict and attenuate free-surface multiples in seismic reflection data (Verschuur, 1992; van Borselen, 1996; Weglein et al., 1997; Ziolkowski et al., 1999; Amundsen, 2001), considerably less attention has been directed toward internal multiple removal. In fact, internal multiple suppression is a relatively recent development in exploration seismology, with the first studies dating from the 1990s.

Araújo et al. (1994) proposed the first data-driven internal multiple elimination method, based on the inverse scattering series (ISS). This method was later developed in more detail in Weglein et al. (1997, 2003). Because ISS was also shown to apply to the elastodynamic wave equation, a similar internal multiple elimination method was extended to work in elastic media by Coates and Weglein (1996), Matson and Weglein (1996), and Matson (1997). Fu and Weglein (2014) applied ISS 1.5D elastic internal multiple attenuation to on-shore field data.

Fokkema et al. (1994) propose a layer-stripping approach to internal multiple removal, based on acoustic reciprocity theorems. Jakubowicz (1998) develops a method based on the feedback model of Verschuur (1992) to predict interbed multiples using correlations within the data, but that method requires that water-bottom-related primaries be identified and isolated. Similarly, Berkhout and Verschuur (1999, 2005) and Verschuur and Berkhout (2005) propose a unified description of internal multiple prediction using the common-focus-point (CFP) approach. To date, however, that theory appears not to have been developed for elastic media.

Although the two main approaches to internal multiple elimination have been described above, an inherently different method has been proposed for acoustic media by Meles et al. (2015). This method makes use of two techniques in exploration seismology: (1) seismic interferometry and (2) Marchenko redatuming. Seismic interferometry uses physical wavefield measurements from real deployed sources to turn real receivers into virtual sources or vice versa (Wapenaar, 2004; van Manen et al., 2005, 2006; Wapenaar and Fokkema, 2006; Curtis et al., 2006, 2009). Marchenko redatuming, on the other hand, uses single-sided reflection data to

Manuscript received by the Editor 29 March 2016; revised manuscript received 22 July 2016; published online 11 January 2017.
[1]The University of Edinburgh, Grant Institute, Edinburgh, UK. E-mail: c.costa@ed.ac.uk; gmeles@staffmail.ed.ac.uk; andrew.curtis@ed.ac.uk.

estimate upgoing and downgoing wavefields at subsurface locations without the need for physical measurements at those virtual locations. Initially developed for acoustic media (Broggini et al., 2012; Wapenaar et al., 2013, 2014), these methods have been extended to elastic media (da Costa Filho et al., 2014; Wapenaar, 2014; Wapenaar and Slob, 2014).

Based on the work of Meles et al. (2015), we propose an elastic, Marchenko-based multiple prediction method, which unites elastic seismic interferometry (Wapenaar, 2004; van Manen et al., 2006) and elastic tensorial Marchenko redatuming (da Costa Filho et al., 2014). Though Marchenko redatuming can be used to estimate the local angle-dependent reflection coefficients in acoustic (Broggini et al., 2014; Slob et al., 2014; Wapenaar et al., 2014) and elastic media (Wapenaar and Slob, 2014; da Costa Filho et al., 2015), that requires Marchenko redatuming to be performed at each depth level at which an estimate is desired. In contrast, our method requires redatuming only to one surface between each pair of internal multiple generators. Furthermore, it does not involve any picking as required in CFP-based methods, nor does it require regularity assumptions on the traveltimes of the multiples as required by ISS (in the form of the so-called lower-higher-lower condition applied in the papers above). We develop the theory below, and then we illustrate it with two synthetic examples.

THEORY

Elastic seismic interferometry prescribes ways in which the elastodynamic Green's functions between two points can be written as convolutions or correlations between Green's functions from or to particular families of closed boundaries. Let $G^{(v,f)}_{(p,q)}(\mathbf{x}_r, \mathbf{x}_s, \omega)$ represent the elastodynamic Green's function in the angular frequency domain ω, measured at $\mathbf{x}_r$ from an impulsive source at $\mathbf{x}_s$. Following the notation of Wapenaar and Fokkema (2006), the first superscript refers to the received quantity (v, τ, ϕ for velocity, stress, and potential, respectively) and the second refers to the emitted quantity (f, h, ϕ for external volume force density, deformation rate density, and potential, respectively). Subscripts represent the components of the received and emitted quantities, respectively. Considering a boundary $\partial\mathbb{D}$, which encloses $\mathbf{x}_r$ but not $\mathbf{x}_s$ (Figure 1a), the following exact relationship can be established (van Manen et al., 2006; Slob et al., 2007) between the elastodynamic Green's functions in the frequency domain:

$$G^{(v,f)}_{(p,q)}(\mathbf{x}_r, \mathbf{x}_s) = \oint_{\partial\mathbb{D}} G^{(v,f)}_{(i,p)}(\mathbf{x}, \mathbf{x}_r) G^{(\tau,f)}_{(ij,q)}(\mathbf{x}, \mathbf{x}_s) - G^{(\tau,f)}_{(ij,p)}(\mathbf{x}, \mathbf{x}_r) G^{(v,f)}_{(i,q)}(\mathbf{x}, \mathbf{x}_s) \mathrm{d}^2\mathbf{x}, \quad (1)$$

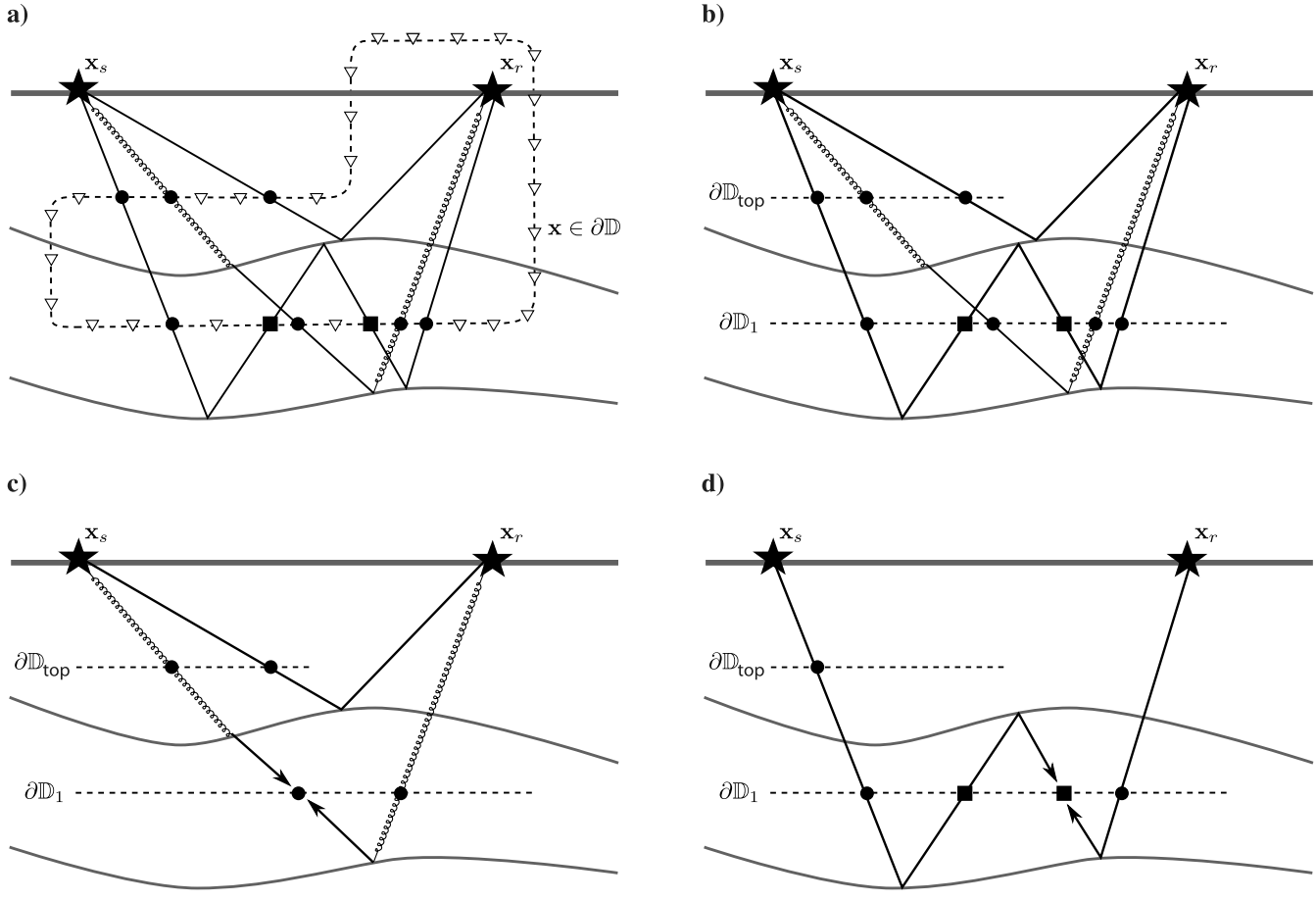

Figure 1. (a) Typical geometry for convolutional interferometry. The closed boundary $\partial\mathbb{D}$ of receivers is represented by a dashed line and white triangles. (b) Geometry with truncated boundaries $\partial\mathbb{D}_{\text{top}}$ and $\partial\mathbb{D}_1$. The $\partial\mathbb{D}_{\text{top}}$ is not used to construct internal multiples. (c) Same geometry as panel (b) showing only the primary. (d) Same geometry as panel (b) showing only the multiple. Solid black lines represent P-waves, and the winding black curves represent S-waves. Stationary points are represented by the solid black squares and circles.

where we have suppressed the frequency dependency to simplify notation and apply the Einstein summation convention for repeated subscripts. Equation 1 is valid for an arbitrarily inhomogeneous anisotropic elastic solid.

From the generalized Hooke's law in the frequency domain and the source-receiver reciprocity relations, we may establish relations analogous to equation 1 with arbitrary velocity or stress receivers, and force or deformation sources. Simply put, the elastic Green's function between two points is obtained by convolving Green's functions from those two points to a boundary of receivers and summing these convolutions over all receivers on the boundary.

The method of stationary phase (Bleistein, 1984) is a method that is commonly used to analyze contributions to interferometric integrals, such as that in equation 1. Works such as that of Snieder et al. (2006) and Slob et al. (2007) show that the main constructively interfering contributions in correlational or convolutional interferometric integrals come from regions around points where the extension of raypaths between points $\mathbf{x}_s$ and $\mathbf{x}_r$ intersects the boundary. Therefore, instead of considering full boundaries, it is enough to have boundaries that sample around these stationary regions. Figure 1a shows a typical geometry for the interferometric integral above, in which we note that the geometry of the closed boundary can be chosen arbitrarily, provided that it encloses only one of $\mathbf{x}_r$ and $\mathbf{x}_s$. The stationary points are shown as solid black circles and squares. It is clear that every stationary point in such a geometry is located along two horizontal parts of the boundary $\partial\mathbb{D}_{\text{top}}$, which is always between the first reflector and the surface, and $\partial\mathbb{D}_j$, which is between reflectors j and $j+1$. Consequently, we may approximate the integrals in equation 1 by considering partial boundaries consisting of open curves (or surfaces, in 3D) in the subsurface, such as shown in Figure 1b.

Along horizontal boundaries, elastodynamic wavefields can be decomposed into upgoing and downgoing components as well as P and S potentials that satisfy one-way equations, provided there are no evanescent or horizontally propagating wave modes (Wapenaar and Haimé, 1990). For example, $G^{(\phi,f)}_{(k,q)}(\mathbf{x},\mathbf{x}_s) = G^{+(\phi,f)}_{(k,q)}(\mathbf{x},\mathbf{x}_s) + G^{-(\phi,f)}_{(k,q)}(\mathbf{x},\mathbf{x}_s)$, where the downgoing (+) and upgoing waves (−) satisfy the following one-way wave equations in the wavenumber-frequency domain:

$$\frac{\partial}{\partial z} G^{\pm(\phi,f)}_{(k,q)}((k_x,k_y,z),\mathbf{x}_s) = \mp\imath\sqrt{\left(\frac{\omega}{c^k}\right)^2 - k_x^2 - k_y^2}\; G^{\pm(\phi,f)}_{(k,q)}((k_x,k_y,z),\mathbf{x}_s), \quad (2)$$

where $\imath$ is the imaginary unit, c^k is the seismic propagation velocity, $(x,y,z)=\mathbf{x}$, and k_x and k_y are the wavenumbers corresponding to x and y, respectively. The P-wave potential is denoted by $k=0$, and $k=1,2,3$ refer to the different polarizations of the S-wave potential. The value c^0 then represents the P-wave propagation velocity, and c^1, c^2, and c^3 represent the variously polarized S-wave propagation velocities.

When integrated along these horizontal boundaries, the contributions of the products of wavefields with the same direction (up-up and down-down) vanish; i.e., they do not contribute energy to the integral. The only products that do are those with opposite directions: up-down and down-up (Wapenaar and Haimé, 1990). Therefore, when we apply receiver-side wavefield decomposition to the fields inside of the integral in equation 1, we obtain

$$G^{(v,f)}_{(p,q)}(\mathbf{x}_r,\mathbf{x}_s) \approx \frac{2}{\rho c^k}\oint_{\partial\mathbb{D}_{\text{top}}\cup\partial\mathbb{D}_j}\{G^{+(\phi,f)}_{(k,p)}(\mathbf{x},\mathbf{x}_r)G^{-(\phi,f)}_{(k,q)}(\mathbf{x},\mathbf{x}_s) + G^{-(\phi,f)}_{(k,p)}(\mathbf{x},\mathbf{x}_r)G^{+(\phi,f)}_{(k,q)}(\mathbf{x},\mathbf{x}_s)\}\mathrm{d}^2\mathbf{x}, \quad (3)$$

where ρ represents the medium density and the superscripts − and + denote upgoing and downgoing wavefields, respectively. Note that the superscript in c^k is not summed.

A study of the stationary points of this integral reveals three interesting observations:

1) Primaries from $\mathbf{x}_s$ to $\mathbf{x}_r$ related to reflectors below depth levels $\partial\mathbb{D}_{\text{top}}$ or $\partial\mathbb{D}_j$ can only be constructed as a combination of a forward-transmitted (nonreflected) wave to the subsurface, and a primary from that point to the surface ($\mathbf{x}_r$). For example, in Figure 1c, the primary from $\mathbf{x}_s$ to $\mathbf{x}_r$ can only be constructed by convolving forward-transmitted waves from $\mathbf{x}_s$ to the black circles and primary reflections from the black circles to $\mathbf{x}_r$, or vice versa.
2) All multiples from $\mathbf{x}_s$ to $\mathbf{x}_r$ may be constructed by combining a forward-transmitted wave from $\mathbf{x}_s$ to a point on one of the boundaries, and a multiple from that point to $\mathbf{x}_r$. For example, in Figure 1d, the multiple may be constructed by convolving forward-transmitted waves from $\mathbf{x}_s$ to the black circles and multiples from the black circles to $\mathbf{x}_r$.
3) Some multiples from $\mathbf{x}_s$ to $\mathbf{x}_r$ may also be constructed by combining a reflected wave from $\mathbf{x}_s$ to a point on $\partial\mathbb{D}_j$, and another reflected wave from that point to $\mathbf{x}_r$. Combining only reflected waves only constructs multiples, specifically, those that have reflected above and below $\partial\mathbb{D}_j$. For example, in Figure 1d, the multiple can be constructed by convolving a multiple from $\mathbf{x}_s$ to a black square and a primary from that black square to $\mathbf{x}_r$.

In light of these observations, we separate the downgoing wavefields in equation 3 with respect to the order of their reflections:

$$G^{(v,f)}_{(p,q)}(\mathbf{x}_r,\mathbf{x}_s) \asymp \frac{2}{\rho c^k}\int_{\partial\mathbb{D}_{\text{top}}\cup\partial\mathbb{D}_j}\Big\{\Big(G^{+(\phi,f)}_{0\,(k,p)}(\mathbf{x},\mathbf{x}_r) + G^{+(\phi,f)}_{M(k,p)}(\mathbf{x},\mathbf{x}_r)\Big)G^{-(\phi,f)}_{(k,q)}(\mathbf{x},\mathbf{x}_s) + G^{-(\phi,f)}_{(k,p)}(\mathbf{x},\mathbf{x}_r)\Big(G^{+(\phi,f)}_{0\,(k,q)}(\mathbf{x},\mathbf{x}_s) + G^{+(\phi,f)}_{M(k,q)}(\mathbf{x},\mathbf{x}_s)\Big)\Big\}\mathrm{d}^2\mathbf{x}, \quad (4)$$

where the subscript 0 denotes no reflection and the subscript M denotes multiple reflections. The upgoing field, which lacks a corresponding subscript, contains primaries and multiples but does not contain nonreflected wavefields. Unlike in acoustic media, wavefields in elastic media that did not undergo any reflections may nevertheless have undergone mode conversions during forward scattering. According to observation 1, primaries in $G^{(v,f)}_{(p,q)}(\mathbf{x}_r,\mathbf{x}_s)$ must necessarily involve $G^{+(\phi,f)}_{0(k,p)}(\mathbf{x},\mathbf{x}_r)$ or $G^{+(\phi,f)}_{0(k,q)}(\mathbf{x},\mathbf{x}_s)$; however, these terms may additionally construct multiples as per observation 2. According to observation 3, terms involving $G^{+(\phi,f)}_{M(k,p)}(\mathbf{x},\mathbf{x}_r)$ or $G^{+(\phi,f)}_{M(k,q)}(\mathbf{x},\mathbf{x}_s)$ necessarily construct only multiples (but not all multiples) in

$G^{(v,f)}_{(p,q)}(\mathbf{x}_r, \mathbf{x}_s)$. Thus, to construct only multiples, we must exclude the terms containing $G^{+(\phi,f)}_{0(k,p)}$. This reasoning leads to a new construction for elastic internal multiples, which reflect above and below the boundary $\partial\mathbb{D}_j$

$$G_{\mathrm{IM}}{}^{(v,f)}_{(p,q)}(\mathbf{x}_r, \mathbf{x}_s) \approx G_{\mathrm{IM_P}}{}^{(v,f)}_{(p,q)}(\mathbf{x}_r, \mathbf{x}_s) + G_{\mathrm{IM_S}}{}^{(v,f)}_{(p,q)}(\mathbf{x}_r, \mathbf{x}_s), \quad (5)$$

where

$$G_{\mathrm{IM_P}}{}^{(v,f)}_{(p,q)}(\mathbf{x}_r, \mathbf{x}_s) = \frac{2}{\rho c^P} \int_{\partial\mathbb{D}_j} \{G^{+(\phi,f)}_{M(P,p)}(\mathbf{x}, \mathbf{x}_r) G^{-(\phi,f)}_{(P,q)}(\mathbf{x}, \mathbf{x}_s) + G^{-(\phi,f)}_{(P,p)}(\mathbf{x}, \mathbf{x}_r) G^{+(\phi,f)}_{M(P,q)}(\mathbf{x}, \mathbf{x}_s)\} \mathrm{d}^2\mathbf{x} \quad (6)$$

and

$$G_{\mathrm{IM_S}}{}^{(v,f)}_{(p,q)}(\mathbf{x}_r, \mathbf{x}_s) = \frac{2}{\rho c^S} \int_{\partial\mathbb{D}_j} \{G^{+(\phi,f)}_{M(S,p)}(\mathbf{x}, \mathbf{x}_r) G^{-(\phi,f)}_{(S,q)}(\mathbf{x}, \mathbf{x}_s) + G^{-(\phi,f)}_{(S,p)}(\mathbf{x}, \mathbf{x}_r) G^{+(\phi,f)}_{M(S,q)}(\mathbf{x}, \mathbf{x}_s)\} \mathrm{d}^2\mathbf{x}, \quad (7)$$

which is equivalent to discarding the circular black stationary points in Figure 1b. As a consequence of discarding these forward transmissions, $\partial\mathbb{D}_{\mathrm{top}}$ never plays a role in constructing the multiples and is therefore not present in equations 5–7. Moreover, according to observation 2, not all multiples are constructed. Therefore, if all multiples are sought, the quantities in equations 5–7 must be summed for multiple boundaries $\partial\mathbb{D}_j$ such that each inter-reflector rock layer contains at least one boundary.

Equations 5–7 can only be applied if one has knowledge of directionally decomposed Green's functions at subsurface points. Although the upgoing field is commonly estimated by backpropagation of the reflected data and the direct downgoing field may be modeled given an approximate or reference velocity model, the multiply scattered downgoing field has been unavailable from conventional redatuming methods. Recently, however, so-called Marchenko methods have been developed, which allow reconstructions of the upgoing and downgoing fields at arbitrary subsurface points, in acoustic (Broggini et al., 2012; Wapenaar et al., 2013, 2014) and elastic media (da Costa Filho et al., 2014, 2015; Wapenaar, 2014; Wapenaar and Slob, 2014). An in-depth account of the Marchenko method is beyond the scope of this paper, but a few observations from the Marchenko-related literature are important here: Marchenko redatuming requires surface-reflection data that are well-sampled in space and time and that have undergone source signature deconvolution. For our elastic Marchenko implementation, the data must be free from source and receiver ghosts as well as free-surface multiples, but this is not a general requirement of Marchenko methods and may be relaxed in the future, if an elastic Marchenko method is developed that accounts for free-surface multiples, as Singh et al. (2015) create for acoustic media. This method also requires an estimate of the P and S forward-scattered wavefield between the surface and subsurface points. In general, smooth velocity models used to compute the direct P- and S-wavefields can be estimated using PP and PS model building techniques. However, estimating the converted transmissions poses a problem because constructing them requires knowledge of the subsurface interfaces. We circumnavigate this limitation by omitting the converted transmissions from the input to the Marchenko method (da Costa Filho et al., 2015), but note that this is known to degrade the reconstructions (Wapenaar and Slob, 2015).

Method

The theoretical considerations described above are used to design a method for elastic internal multiple estimation. The method consists of the following four steps:

1) Define a horizontal boundary $\partial\mathbb{D}_j$ at a chosen subsurface depth. For a set of sample locations along $\partial\mathbb{D}_j$, use the direct P- and S-waves from the smooth velocity models to estimate the up- and downgoing fields $G^{+/-(\phi,\cdot)}_{(N,\cdot)}(\mathbf{x}, \mathbf{x}_{r/s})$ using Marchenko methods.
2) Mute the direct waves in the estimated downgoing wavefields. This can be done by windowing the wavefield based on the direct-wave arrival traveltimes. If there are any other artifacts in the up- or downgoing Green's functions, these must also be removed.
3) Apply equations 5–7 using the fields obtained in the previous step to estimate the internal multiples $G_{\mathrm{IM}}{}^{(\cdot,\cdot)}_{(\cdot,\cdot)}(\mathbf{x}_r, \mathbf{x}_s)$ for each source/receiver combination.
4) Repeat steps 1–3 for boundary $\partial\mathbb{D}_j$ at each depth level to construct the multiples associated with reflectors beneath that level.

The algorithm proposed above can be used to estimate and to remove multiples. Meles et al. (2015) stack the results from each depth level and then adaptively subtract the multiples from each common-shot gather (CSG). Here, we propose stacking all terms containing P-wave subsurface receivers (equation 6) separately from those containing S-wave subsurface receivers (equation 7). These two separate quantities are adaptively subtracted (Fomel, 2009) from the data in the common-offset gather (COG) sequentially: First is the P-wave contribution and then S. The subtractions are then repeated in reverse order. Finally, these two results are averaged.

We do not simply stack all gathers because to sum them, one must know the subsurface P- and S-wave velocities (see equations 6 and 7), and although their estimates are usually available, they might not be sufficiently accurate for amplitude weighting. Another issue is that direct P- and S-waves must involve accurate relative amplitudes between the P and S sources, which might also be unavailable. Our sequential stacking approach solves both of those issues. In fact, amplitudes will, in the general case, contain errors because each partial boundary $\partial\mathbb{D}_j$ produces a subset of the multiples, so when the results are stacked, some multiples will be enhanced by stacking multiple copies, whereas others will not.

We use COGs for adaptive subtraction because events are less likely to cross in the COGs than in CSGs for models that are approximately horizontally layered. Multiples may also be identified in prestack and migrated sections.

As opposed to acoustic media in which there is only one direct wave, in elastic media, there are several forward-scattered events that may construct primaries. All of these must be removed in step 2, so that primaries are not reconstructed. Using only the P and S direct waves in the Marchenko method guarantees that those will be the only two forward-scattered events present, and therefore, their removal is enough to ensure no primaries are constructed. However, as is known from Wapenaar and Slob (2015), this approximation leads to artifacts in the reconstructed fields. These artifacts will not create primaries, but they may construct spurious multiples. In our examples, we muted the upgoing and downgoing gathers before the last-arriving direct-wave energy ensuring artifact-free internal multiple estimates.

NUMERICAL EXAMPLES

Layered model

The model used for the first data set had a horizontally layered density profile (Figure 2) and constant P and S velocities of 2.5 and 1.3 km/s, respectively.

The Marchenko method requires reflection data to be recorded with a wide band, wide aperture, and densely sampled seismic acquisition system with colocated sources and receivers that have undergone removal of the direct wave, source or receiver ghosts, surface-related multiples, and ground roll. In these numerical examples, we used finite-difference modeling (Virieux, 1986) with absorbing boundary conditions surrounding the medium, thus producing no ghosts or surface-related phenomena. Receivers and sources were colocated at every 10 m from 200 to 1800 m. To remove the direct wave, we subtracted from it the gathers acquired from a model with constant density and hence no interfaces. Finally, the data underwent source wavelet deconvolution.

To obtain all of the internal multiples, the method only needed to be applied using two depths, which we chose to be at 250 and 650 m (Figure 2). In step 1 of the method, we calculated up- and downgoing P- and S-wavefields at subsurface points along each depth using the elastic Marchenko method described in da Costa Filho et al. (2015). In step 2, we muted the direct wave from the up- and downgoing fields and performed f-k filtering to remove unwanted artifacts produced by the Marchenko method. We illustrate in Figure 3 the first two steps at a virtual receiver on the topmost boundary $\partial\mathbb{D}_1$. At lateral position 1200 m, we estimate the receiver-side P-wave potential from a vertical force source. The f-k filtered down- and upgoing potentials are shown in Figure 3a and 3b, respectively. Also shown in Figure 3 is the window used in step 2 to remove the direct wave.

In step 3, we applied equations 6 and 7 to obtain the P- and S-wave subsurface contributions to the internal multiples. The CSGs of these are shown in Figure 4c and 4d, and can be compared to a CSG from the original data as shown in Figure 4a. The gather in Figure 4c contains all PP reflections, whereas the gather in Figure 4d contains all SS reflections. Conversions will appear in both gathers because they may be constructed using either up- and downgoing P-waves or up- and downgoing S-waves, e.g., the bottom-most arrow in Figure 4c and 4d. This is seen in Figure 5, which shows how a converted event can be constructed from convolving two singly reflected events: on the left involving P receiver-side potentials, and on the right involving S receiver-side potentials. These internal multiples were adaptively subtracted from the original data yielding the demultipled data, as shown in Figure 4b. All multiples have been accurately predicted, and they have been reasonably attenuated in the gather as shown by arrows in Figure 4.

To further verify the results, we generate PP and SS images using conventional migration. For PP images, we used the vertical particle velocity from vertical force sources; whereas for SS images, we used the horizontal particle velocity from horizontal force sources. The PP images from the original and demultipled data are shown in Figure 6a and 6b, respectively, whereas the SS images from the original and demultipled data are shown in Figure 7a and 7b, respectively. The images formed by the demultipled data have greatly reduced artifacts, compared with the images from the original data, which display numerous artifacts (arrows in Figures 6a and 7a). We also show the image produced by migrating only the predicted multiples, the P-multiples being imaged in Figure 6c and the S-multiples in Figure 7c. Both are in kinematic agreement with the multiply reflected spurious reflectors in the images from the original data. We therefore conclude that for this simple layered model, the algorithm has performed well.

Complex model

To test the method in a more challenging solid-earth-type scenario, we used a model that contained a significant anticline with added stochastically generated vertical and horizontal heterogeneities in density, P-wave velocity, and S-wave velocity. Density and P-wave velocities are shown in Figure 8; S-wave velocity is set at 0.85 km/s in the first layer, and it is calculated with the formula

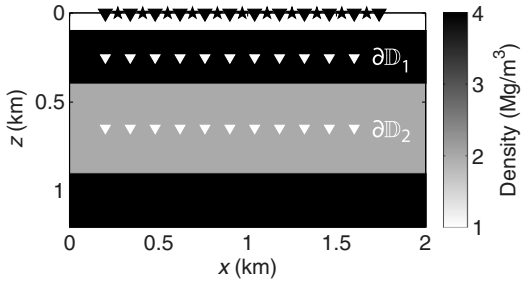

Figure 2. Density profile of the layered model. Black stars and triangles represent colocated surface sources and receivers; white triangles represent chosen boundaries $\partial\mathbb{D}_1$ and $\partial\mathbb{D}_2$.

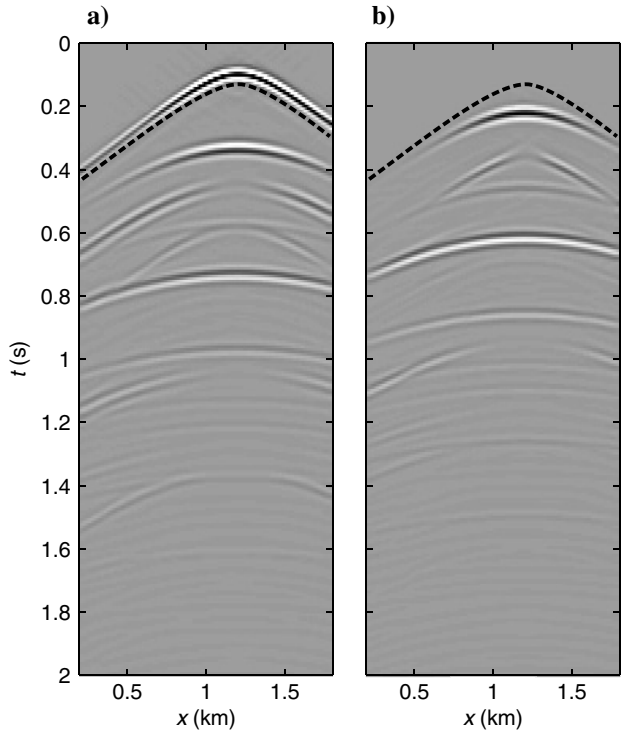

Figure 3. Subsurface (a) downgoing and (b) upgoing P-wave potentials estimated with the Marchenko method at (1200 m, 250 m) (on boundary $\partial\mathbb{D}_1$). Both gathers originate from vertical force sources at the surface and have been f-k filtered. Dashed lines show the last arriving energy of the direct P-wave, before which both gathers will be muted.

$V_S = 0.5832V_P - 0.0777$ for the subsequent depths (Castagna et al., 1993). The data were modeled and preprocessed similarly to the previous layered model, using finite-difference modeling with absorbing boundary conditions with sources and receivers spaced 12 m apart from 0 to 2.4 km.

In step 1, we chose three depth levels between the multiple generating boundaries to place virtual receivers as in Figure 8. Using a smooth model (not shown), we computed the direct arrivals to these virtual receivers, and we subsequently used the Marchenko method to calculate the up- and downgoing fields at each of these locations. In step 2, we muted the forward-scattered arrivals from these fields. In step 3, the prestack gathers of estimated internal multiples are obtained.

The CSGs are shown in Figure 9. The original data are shown in Figure 9a and contain many primaries and complex internal multiples. We show the corresponding demultipled gather in Figure 9b as well as the P and S internal multiple gathers in Figure 9c and 9d. The dashed boxes in Figure 9 enclose a region that is magnified in Figure 10. In this figure, we observe that the original data (Figure 10a) contain many internal multiples as indicated by the arrows. These are reasonably attenuated in the demultipled gather (Figure 10b).

To test the effect on imaging, we migrated the original data, the demultipled data, and the P and S internal multiples using dynamically correct elastic RTM (Ravasi and Curtis, 2013). The result of the PP imaging is shown in Figure 11. Figure 11a shows the migrated original data, which contains the true reflectors imaged correctly (solid curves), but it also displays many spurious reflectors generated by internal multiples, some of which are indicated by the solid arrows. Figure 11b shows the migrated demultipled data: True reflectors are more prominent because some of the internal multiples have been correctly attenuated and primaries have been preserved — the arrows indicate two strong spurious reflectors that were attenuated. These spurious reflectors can be seen clearly in Figure 11c, which shows the migrated P internal multiples. As expected, this image contains no true reflectors, but it is potentially extremely useful because it identifies internal multiple-related artifacts that are present in the original imaging panel (Figure 11a). For example, both structures indicated by arrows in Figure 11a also exist in Figure 11c, and this shows that they are likely to be the result of migrating multiples.

The SS-wave migrated images using the original S-wave gathers, the demultipled gathers, and the image from migrating S internal multiples are shown in Figure 12a–12c, respectively. Again, migrating the original gathers creates true but also spurious structures due to internal multiples, the strongest of which are indicated by the arrows. These are significantly attenuated in the demultipled image, which features no strong internal multiple-related artifacts. However, also the primaries appear weaker, an indication that the adaptive subtraction has been too severe, deteriorating primary energy. The demultipled image also shows incoherent artifacts above the top reflector; these are also caused by the adaptive subtraction, as can be seen by the deterioration in the S-waves outside of the

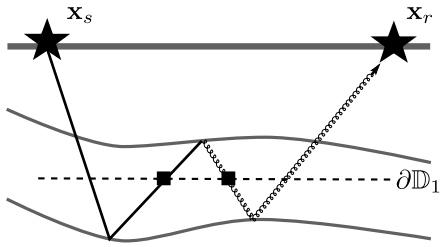

Figure 5. Internal multiple constructed by two stationary points. Stationary point on the left combines P-wave energy, and the one on the right combines S-wave energy. Key as in Figure 1.

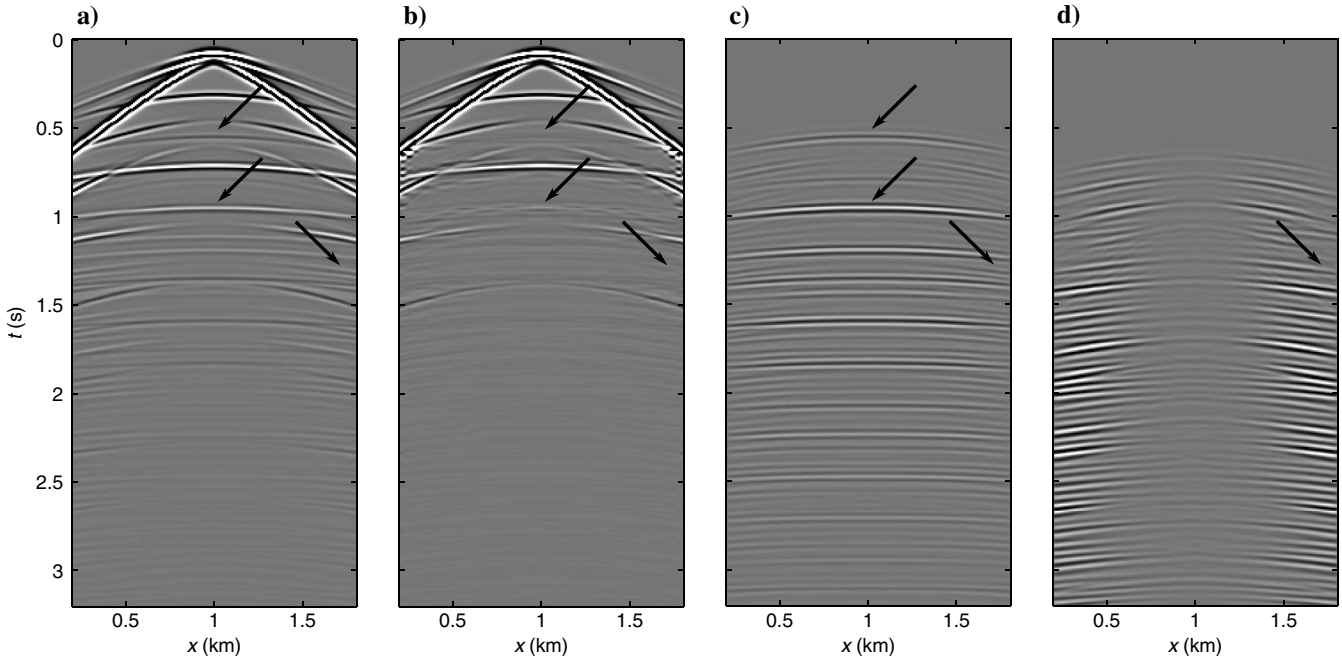

Figure 4. CSGs from the layered model of the (a) original data and (b) demultipled data. Also, predicted multiples using (c) P-wave subsurface receivers and (d) S-wave subsurface receivers. The quantity shown is the vertical particle velocity from a vertical force source. Arrows indicate specific multiple events that appear in panel (a, c, or d), but that have been attenuated in panel (b).

box in Figure 9b. Note that neither Figure 12a nor Figure 12c exhibits these because the gathers in Figure 9a and 9c do not suffer this deterioration. Despite this, the spurious S-reflections in Figure 12c show a fairly good mapping of where internal multiples are present in the original image.

Complex model — Pseudoacoustic approximation

The full-elastic theory presented herein requires knowledge or accurate estimation of wavefield components not usually available from standard seismic acquisitions. Therefore, it is of interest to evaluate the performance of the method when lacking many of these components. We reduce the (in 2D) 16-component elastic tensor to only one of its components, namely, $G^{-(v,f)}_{(z,z)}$, and we use it to perform the acoustic version of the method given in Meles et al. (2015). This can be seen as a pseudoacoustic approximation to the elastic method (see Appendix C of da Costa Filho et al., 2015).

Figure 13 shows a section of CSGs of the single-component original data, the predicted multiples using the pseudoacoustic method, and the demultipled gather obtained by adaptively subtracting the multiples from the original data. Multiples in Figure 13c show the same kinematic behavior as the true multiples in the original data in Figure 13a, as indicated by white arrows. Although some artifacts do appear (black arrow), primaries in the demultipled data (Figure 13b) do not seem to be harmed. This may be explained by the fact that the artifacts have different moveout than true events, and the adaptive subtraction requires continuity along time and space.

We migrate the data using acoustic RTM, as shown in Figure 14. As expected from the analysis of the CSGs, multiples are well-estimated by the pseudoacoustic method, as shown in Figure 14c. Moreover, the artifacts seen in the CSG do not appear to be coherently imaged. The migration of the demultipled data shows attenuated multiples, as indicated by the white arrows in Figure 14b. However, different from the elastic imaging, some true reflectors have also been attenuated. Nevertheless, the results show that even given the dramatic reduction in the number of components used, multiples can still be effectively estimated and attenuated in elastic data using acoustic processing.

DISCUSSION

It is clear from the results shown in the previous sections that the method may be a useful tool to identify internal multiples in pre-

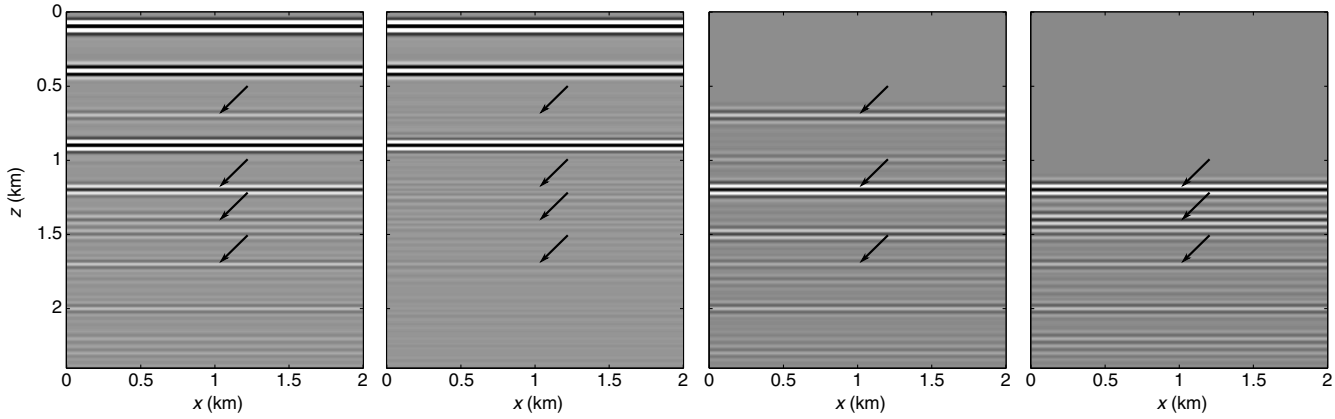

Figure 6. The PP images using (a) the original data, (b) the demultipled data, (c) the P-multiples generated using the first boundary, and (d) the P-multiples using the second boundary in Figure 2. Arrows show some prominent multiple-generated artifacts. Images in panels (a and b) have the same scale, and all images are gained proportionally to depth to highlight deeper structures.

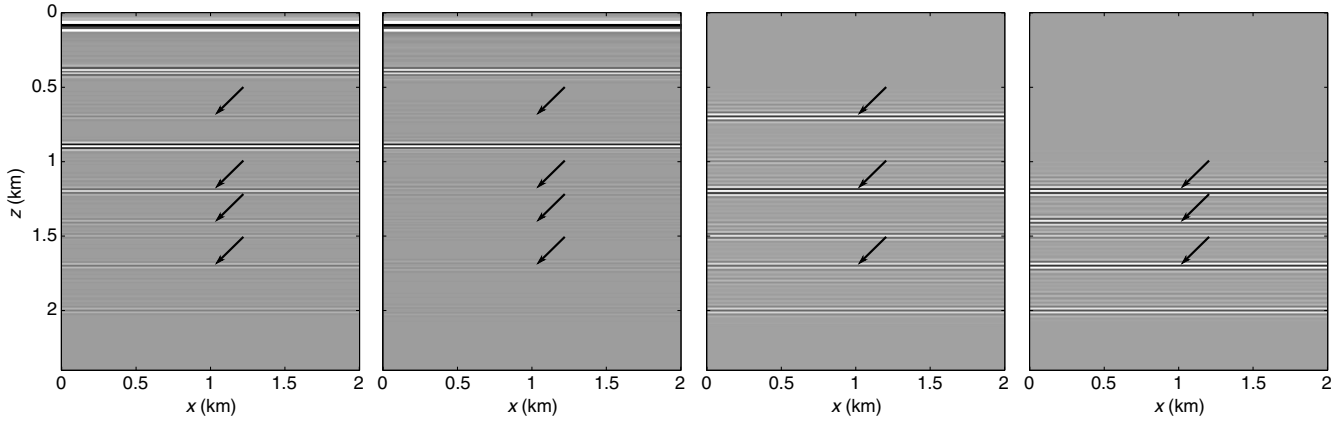

Figure 7. The SS images using (a) the original data, (b) the demultipled data, (c) the S-multiples generated using the first boundary, and (d) the S-multiples generated the second boundary in Figure 6. Key as in Figure 6.

stack data as well as in migrated images. It is also flexible enough that one may choose to generate only a subset of multiples by selecting specific depth levels and polarities (e.g., only P or only S). The choice of depth levels is important, and it may be made in several ways. Meles et al. (2015, 2016) discuss the benefits and drawbacks of selecting regularly spaced horizontal boundaries. Another choice is to manually or automatically select level curves of the velocity model. We propose yet another manner, which guarantees one boundary per layer.

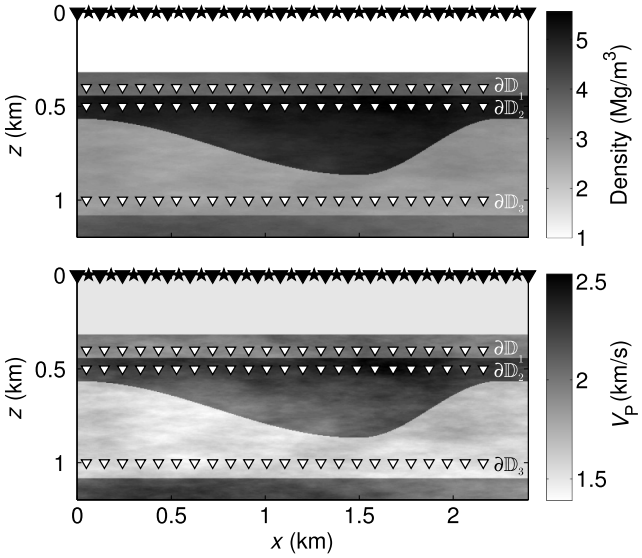

Figure 8. Densities and P velocities of the complex model. There are large-scale density and velocity contrasts creating discrete interfaces as well as small-scale heterogeneities that distort wavefronts. Key as in Figure 2.

After imaging the original data set, one interprets every event as a true reflector and places boundaries in between each of those events. For example, in our first model, we may initially choose depth levels between each apparent interface in Figure 6a. Starting from the top, we may choose a boundary at depth 250 m, which lies between the first two apparent interfaces to calculate multiples. Then, we move on to the next depth level at 650 m, which lies between the second and third apparent reflectors. As shown in Figure 6, the multiple contributions from the boundary at 250 m (Figure 6c) are different from those from the boundary at 650 m (Figure 6d); therefore, we are correct in supposing that there is one reflecting interface separating the two boundaries and both boundaries must therefore be used. This comparison need not to be done in the image space: For example, the prestack multiples constructed from the boundary at 650 m are exactly the same as those constructed from the boundary at 750 m, as is shown in Figure 15. We conclude that the apparent reflector separating them is spurious, and thus only one of those boundaries is needed. Finally, choosing a depth level at 1000 m does not construct any multiples at all because no reflector exists below that depth. Thus, no more boundaries are needed, and in fact, only those at depths 250 and 650 m contribute all possible multiples.

In spite of efforts to guarantee only one boundary per layer, the nature of stacking multiples from different depth levels intrinsically oversamples some multiples. This is illustrated by Figure 16, which shows that boundaries at different depths construct some of the same multiples. In fact, this was observed in the first model, where some migrated multiples from the first boundary (Figure 6c) also appear in the migrated multiples from the second boundary (Figure 6d). This causes multiples to be constructed with incorrect rel-

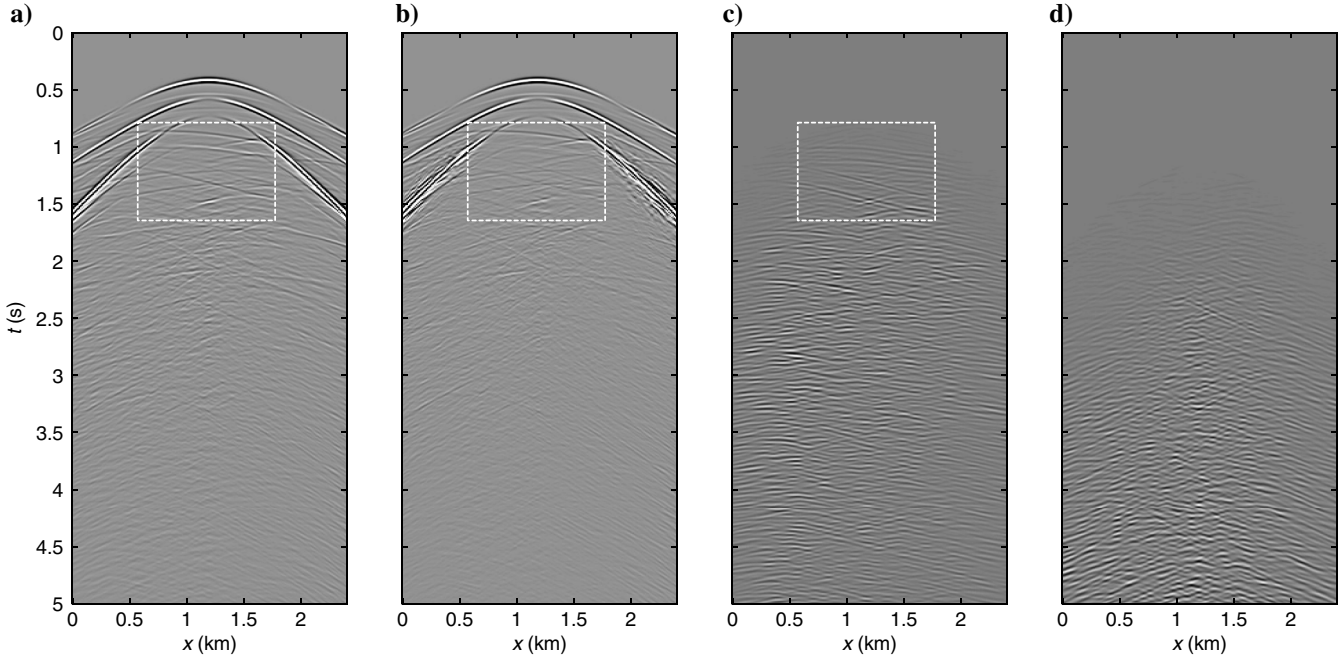

Figure 9. CSGs from the complex model of (a) the original data and (b) the demultipled data. Also shown are the predicted multiples using (c) P-wave subsurface receivers and (d) S-wave subsurface receivers. The quantity shown is the vertical particle velocity from a vertical force source. The dotted lines bound the region magnified in Figure 10.

ative amplitudes. Additionally, shortcomings in the interferometric integrals (equations 5–7), such as incomplete boundaries and the removal of the direct wave in the convolution, introduce further amplitude errors in the construction of multiples. Consequently, if multiple elimination is the goal, proper adaptive subtraction methods are paramount. Although we have obtained reasonable results in

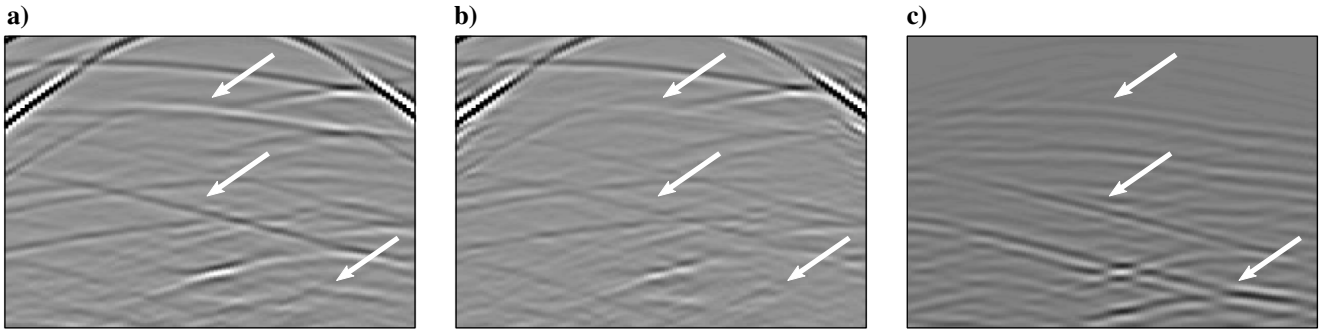

Figure 10. Magnified portion of the CSGs in Figure 9 of (a) the original data and (b) the demultipled data. Also shown are the (c) predicted multiples using P-wave subsurface receivers.

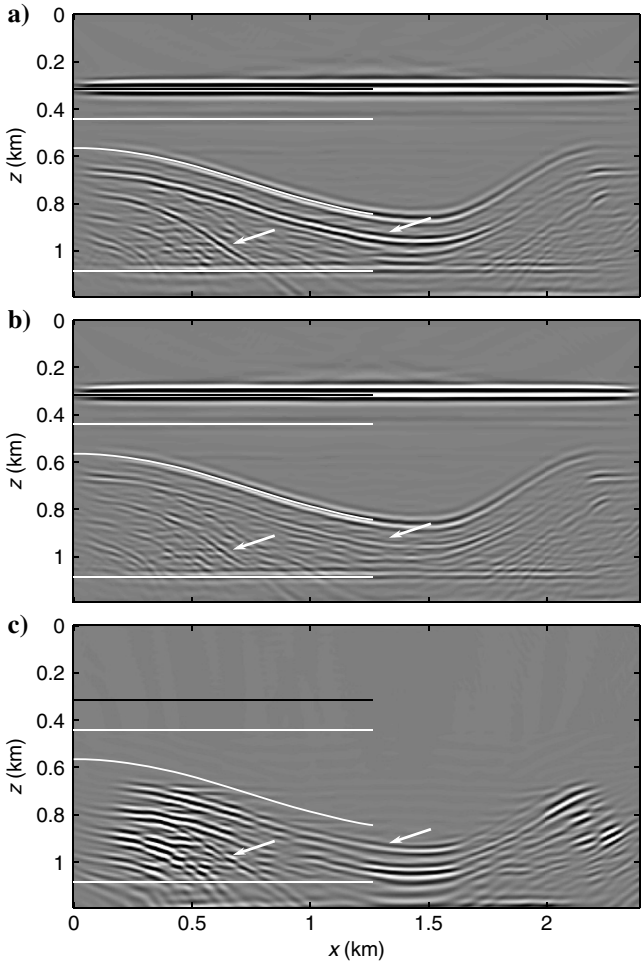

Figure 11. The PP images from dynamically correct elastic RTM of (a) the original data, (b) the demultipled data, and (c) the predicted multiples using P-wave subsurface virtual receivers. All images have had a gain proportional to depth applied to enhance lower reflectors. Panels (a and b) have the same scale and have undergone low-frequency artifact removal by Laplacian filtering. Solid white and black lines denote the position of the true interfaces. White arrows point to multiple-related artifacts.

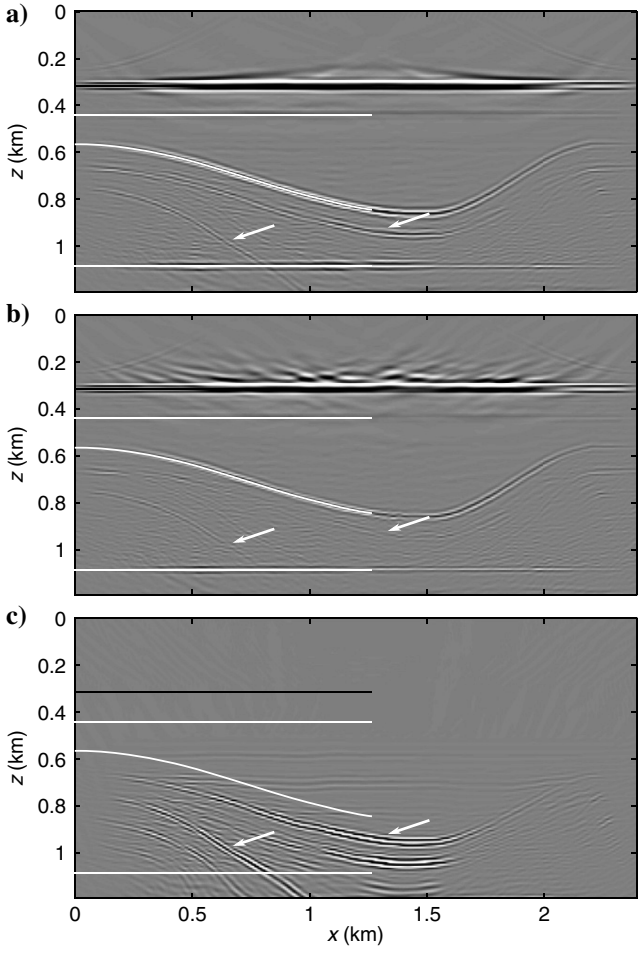

Figure 12. The SS images from dynamically correct elastic RTM of (a) the original data, (b) the demultipled data, and (c) the predicted multiples using S-wave subsurface virtual receivers. All images have had a gain proportional to depth applied to enhance lower reflectors. Panels (a and b) have the same scale and have undergone low-frequency artifact removal. Solid white and black lines denote the position of the true interfaces. White arrows point to multiple-related artifacts.

our numerical examples, further study is needed to characterize its efficiency in more complex data sets. Nevertheless, we have shown how well multiples are recovered kinematically and how this impacts internal multiple identification in the prestack and migrated data. Furthermore, certain families of multiples may be missed if no boundaries are placed between two multiple generators. As with

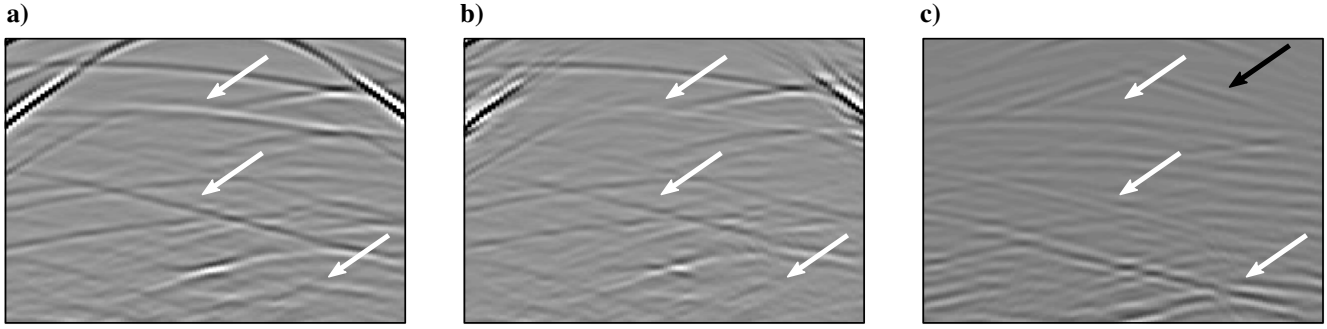

Figure 13. The same magnified portion of the data as in Figure 9: (a) the original data, (b) the demultipled data using the pseudoacoustic method, and (c) the predicted multiples using the pseudoacoustic method. White arrows indicate multiples, and the black arrow indicates an artifact.

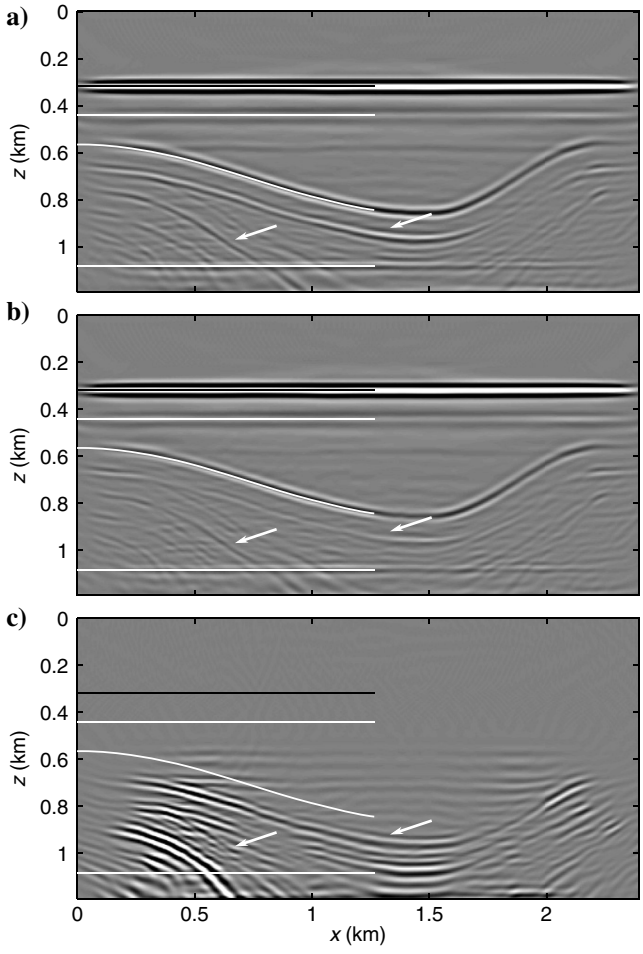

Figure 14. The PP images from acoustic RTM of (a) the original data, (b) the demultipled data using the pseudoacoustic multiples, and (c) the predicted multiples using the pseudoacoustic method. All images have had a gain proportional to depth applied to enhance lower reflectors. Panels (a and b) have the same scale and have undergone low-frequency artifact removal by Laplacian filtering. Solid white and black lines denote the position of the true interfaces. White arrows point to multiple-related artifacts.

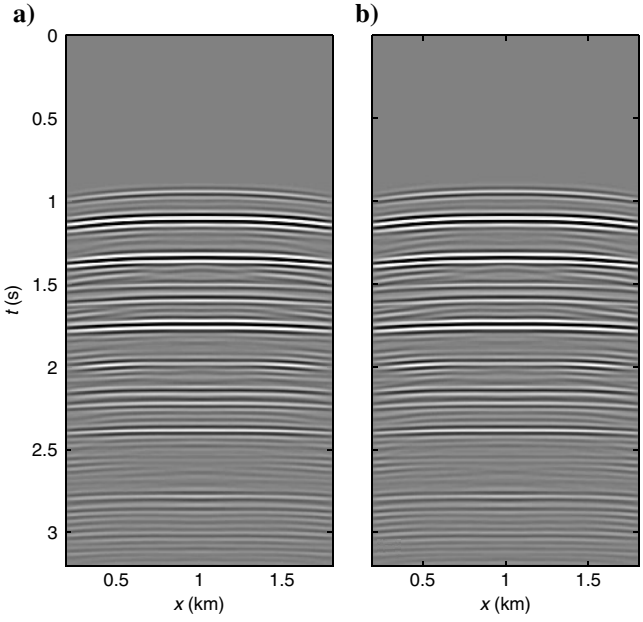

Figure 15. CSGs from the layered model of the P-wave subsurface receivers at (a) 650 and (b) 750 m.

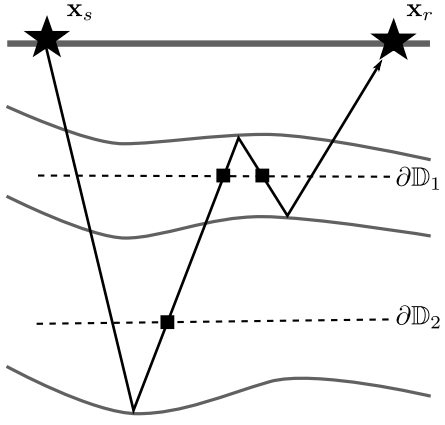

Figure 16. Internal multiple constructed by two boundaries in different layers. Key as in Figure 1.

the excess of boundaries, there is no a priori remedy to insufficient boundaries; one solution is to progressively increase the number of boundaries until no new multiples are generated.

Experiments in the complex elastic model using an acoustic approximation to the full multiple-prediction method suggest that the method can still be useful even when the full elastic tensor is not available, as is often the case in seismic exploration. Results show that multiples are properly constructed with minor artifacts in prestack data and are migrated to correct locations in the image. In fact, all pseudoacoustic migrations in Figure 14 show images with fewer artifacts than their elastic counterparts in Figure 11. This may be explained by the fact that the elastic data contain strong S-waves in the horizontal components, which are not entirely mitigated in the migration. This is especially true in the elastic demultipled data because the adaptive subtraction affects amplitudes, which otherwise might result in a perfect cancellation of events. On the other hand, the images obtained with acoustic RTM show markedly lower resolution than the elastic images; the lack of S-waves limits the resolution of the pseudoacoustic migration. However, in areas where S-wave contribution is significant, such as under gas clouds, adaptively subtracting S-wave multiples may harm P-wave primaries. The pseudoacoustic approximation may possibly prove advantageous in these scenarios, though future work is needed to confirm this.

The image obtained by migrating the pseudoacoustic demultipled data (Figure 14b) also shows slightly attenuated true reflectors. This may be caused by the artifacts that arise from the approximate Marchenko method. Nevertheless, the pseudoacoustic application of the method shows that even in the case with a severely limited number of elastic components (reduced to only one in these experiments), multiple estimation and attenuation are still possible and offer satisfactory results.

CONCLUSION

We present a method to estimate internal multiples in prestack elastic reflection data, based on convolutional interferometry and the elastic Marchenko Green's function construction method. It consists of computing up- and downgoing elastic Green's functions from receivers at the surface to virtual receivers at certain depths, windowing them, and using convolutional interferometry to obtain gathers that only contain internal multiples. The method requires no detailed knowledge of subsurface reflectors, and it only requires a smooth macromodel of P and S velocities similar to that used in migration. We apply the method to two numerical models: one containing only horizontal density interfaces, and another with horizontal and vertical density and velocity variations. We demonstrate how the method can be used to demultiple prestack data, as well as to identify internal multiples in prestack data and their associated spurious reflectors in migrated data. We also evaluate how the elastic method compares to using the acoustic method on a single component of the data. We show that even in this situation, internal multiples may be generated and attenuated with relatively minor side effects.

ACKNOWLEDGMENTS

The authors thank the Edinburgh Interferometry Project sponsors (ConocoPhillips, Schlumberger Gould Research, as well as Statoil and Total) for supporting this research. The first author would like to thank CAPES for research funding. The authors also thank assistant editor J. Shragge, two anonymous reviewers, and D.-J. van Manen for their suggestions.

REFERENCES

Amundsen, L., 2001, Elimination of free-surface related multiples without need of the source wavelet: Geophysics, **66**, 327–341, doi: 10.1190/1.1444912.

Araújo, F. V., A. B. Weglein, P. M. Carvalho, and R. H. Stolt, 1994, Inverse scattering series for multiple attenuation: An example with surface and internal multiples: 64th Annual International Meeting, SEG, Expanded Abstracts, 1039–1041.

Berkhout, A. J., and D. J. Verschuur, 1999, Removal of internal multiples: 69th Annual International Meeting, SEG, Expanded Abstracts, 1334–1337.

Berkhout, A. J., and D. J. Verschuur, 2005, Removal of internal multiples with the common-focus-point (CFP) approach — Part 1: Explanation of the theory: Geophysics, **70**, no. 3, V45–V60, doi: 10.1190/1.1925753.

Bleistein, N., 1984, Mathematical methods for wave phenomena: Academic Press, Inc.

Broggini, F., R. Snieder, and K. Wapenaar, 2012, Focusing the wavefield inside an unknown 1D medium: Beyond seismic interferometry: Geophysics, **77**, no. 5, A25–A28, doi: 10.1190/geo2012-0060.1.

Broggini, F., R. Snieder, and K. Wapenaar, 2014, Data-driven wavefield focusing and imaging with multidimensional deconvolution: Numerical examples for reflection data with internal multiples: Geophysics, **79**, no. 3, WA107–WA115, doi: 10.1190/geo2013-0307.1.

Castagna, J. P., M. L. Batzle, and T. K. Kan, 1993, Rock physics: The link between rock properties and AVO response, *in* J. Castagna, and M. Backus, eds., Offset-dependent reflectivity: Theory and practice of AVO analysis: SEG Investigations in Geophysics 8, 135–171.

Coates, R. T., and A. B. Weglein, 1996, Internal multiple attenuation using inverse scattering: Results from prestack 1D & 2D acoustic and elastic synthetics: 66th Annual International Meeting, SEG, Expanded Abstracts, 1522–1525.

Curtis, A., H. Nicolson, P. Gerstoft, H. Sato, R. Snieder, and K. Wapenaar, 2006, Seismic interferometry — Turning noise into signal: The Leading Edge, **25**, 1082–1092, doi: 10.1190/1.2349814.

Curtis, A., H. Nicolson, D. Halliday, J. Trampert, and B. Baptie, 2009, Virtual seismometers in the subsurface of the earth from seismic interferometry: Nature Geoscience, **2**, 700–704, doi: 10.1038/ngeo615..

da Costa Filho, C. A., M. Ravasi, and A. Curtis, 2015, Elastic P- and S-wave autofocus imaging with primaries and internal multiples: Geophysics, **80**, no. 5, S187–S202, doi: 10.1190/geo2014-0512.1.

da Costa Filho, C. A., M. Ravasi, A. Curtis, and G. A. Meles, 2014, Elastodynamic Green's function retrieval through single-sided Marchenko inverse scattering: Physical Review E, **90**, 063201, doi: 10.1103/PhysRevE.90.063201.

Feldman, M., S. Katyal, and M. Blackwood, 2009, US artifacts: Radiographics, **29**, 1179–1189, doi: 10.1148/rg.294085199.

Fokkema, J. T., R. Van Borselen, and P. Van den Berg, 1994, Removal of inhomogeneous internal multiples: 56th Annual International Conference and Exhibition, EAGE, Extended Abstracts, H039.

Fomel, S., 2009, Adaptive multiple subtraction using regularized nonstationary regression: Geophysics, **74**, no. 1, V25–V33, doi: 10.1190/1.3043447.

Fu, Q., and A. B. Weglein, 2014, Internal multiple attenuation on Encana data: 84th Annual International Meeting, SEG, Expanded Abstracts, 4118–4123.

Jakubowicz, H., 1998, Wave equation prediction and removal of interbed multiples: 68th Annual International Meeting, SEG, Expanded Abstracts, 1527–1530.

Matson, K. H., 1997, An inverse scattering series method for attenuating elastic multiples from multicomponent land and ocean bottom seismic data: Ph.D. thesis, The University of British Columbia.

Matson, K., and A. B. Weglein, 1996, Removal of elastic interface multiples from land and ocean bottom data using inverse scattering: 66th Annual International Meeting, SEG, Expanded Abstracts, 1526–1530.

Meles, G. A., K. Löer, M. Ravasi, A. Curtis, and C. A. da Costa Filho, 2015, Internal multiple prediction and removal using Marchenko autofocusing and seismic interferometry: Geophysics, **80**, no. 1, A7–A11, doi: 10.1190/geo2014-0408.1.

Meles, G. A., K. Wapenaar, and A. Curtis, 2016, Reconstructing the primary reflections in seismic data by Marchenko redatuming and convolutional interferometry: Geophysics, **81**, no. 2, Q15–Q26, doi: 10.1190/geo2015-0377.1.

Ravasi, M., and A. Curtis, 2013, Elastic imaging with exact wavefield extrapolation for application to ocean-bottom 4C seismic data: Geophysics, **78**, no. 6, S265–S284, doi: 10.1190/geo2013-0152.1.

Singh, S., R. Snieder, J. Behura, J. van der Neut, K. Wapenaar, and E. Slob, 2015, Marchenko imaging: Imaging with primaries, internal multiples, and free-surface multiples: Geophysics, **80**, no. 5, S165–S174, doi: 10.1190/geo2014-0494.1.

Slob, E., D. Draganov, and K. Wapenaar, 2007, Interferometric electromagnetic Green's functions representations using propagation invariants: Geophysical Journal International, **169**, 60–80, doi: 10.1111/j.1365-246X.2006.03296.x.

Slob, E., K. Wapenaar, F. Broggini, and R. Snieder, 2014, Seismic reflector imaging using internal multiples with Marchenko-type equations: Geophysics, **79**, no. 2, S63–S76, doi: 10.1190/geo2013-0095.1.

Snieder, R., K. Wapenaar, and K. Larner, 2006, Spurious multiples in seismic interferometry of primaries: Geophysics, **71**, no. 4, SI111–SI124, doi:.doi: 10.1190/1.2211507.

Taheri, A., and F. Honarvar, 2016, Multiple scattering of an acoustic wave from a network of cylindrical rods encased in a solid viscoelastic medium: Ultrasonics, **64**, 69–76, doi: 10.1016/j.ultras.2015.07.015.

van Borselen, R. G., 1996, Removal of surface-related wave phenomena: The marine case: Geophysics, **61**, 202–210, doi: 10.1190/1.1443940.

van Manen, D.-J., A. Curtis, and J. O. A. Robertsson, 2006, Interferometric modeling of wave propagation in inhomogeneous elastic media using time reversal and reciprocity: Geophysics, **71**, no. 4, SI47–SI60, doi: 10.1190/1.2213218.

van Manen, D.-J., J. O. A. Robertsson, and A. Curtis, 2005, Modeling of wave propagation in inhomogeneous media: Physical Review Letters, **94**, 164301, doi: 10.1103/PhysRevLett.94.164301.

Verschuur, D. J., 1992, Adaptive surface-related multiple elimination: Geophysics, **57**, 1166–1177, doi: 10.1190/1.1443330.

Verschuur, D. J., and A. J. Berkhout, 2005, Removal of internal multiples with the common-focus-point (CFP) approach — Part 2: Application strategies and data examples: Geophysics, **70**, no. 3, V61–V72, doi: 10.1190/1.1925754.

Virieux, J., 1986, P-SV wave propagation in heterogeneous media: Velocity-stress finite-difference method: Geophysics, **51**, 889–901, doi: 10.1190/1.1442147.

Wapenaar, K., 2004, Retrieving the elastodynamic Green's function of an arbitrary inhomogeneous medium by cross correlation: Physical Review Letters, **93**, 254301, doi: 10.1103/PhysRevLett.93.254301.

Wapenaar, K., 2014, Single-sided Marchenko focusing of compressional and shear waves: Physical Review E, **90**, 063202, doi: 10.1103/PhysRevE.90.063202.

Wapenaar, K., F. Broggini, E. Slob, and R. Snieder, 2013, Three-dimensional single-sided Marchenko inverse scattering, data-driven focusing, Green's function retrieval, and their mutual relations: Physical Review Letters, **110**, 0843011, doi: 10.1103/PhysRevLett.110.084301.

Wapenaar, K., and J. T. Fokkema, 2006, Green's function representations for seismic interferometry: Geophysics, **71**, no. 4, SI33–SI46, doi: 10.1190/1.2213955.

Wapenaar, C. P. A., and G. C. Haimé, 1990, Elastic extrapolation of primary seismic P- and S-waves: Geophysical Prospecting, **38**, 23–60, doi: 10.1111/j.1365-2478.1990.tb01833.x.

Wapenaar, K., and E. Slob, 2014, On the Marchenko equation for multicomponent single sided reflection data: Geophysical Journal International, **199**, 1367–1371, doi: 10.1093/gji/ggu313.

Wapenaar, K., and E. Slob, 2015, Initial conditions for elastodynamic Green's function retrieval by the Marchenko method: 85th Annual International Meeting, SEG, Expanded Abstracts, 5074–5080.

Wapenaar, K., J. Thorbecke, J. van der Neut, F. Broggini, E. Slob, and R. Snieder, 2014, Marchenko imaging: Geophysics, **79**, no. 3, WA39–WA57, doi: 10.1190/geo2013-0302.1.

Weglein, A. B., F. V. Araújo, P. M. Carvalho, R. H. Stolt, K. H. Matson, R. T. Coates, D. Corrigan, D. J. Foster, S. A. Shaw, and H. Zhang, 2003, Inverse scattering series and seismic exploration: Inverse Problems, **19**, R27–R83, doi: 10.1088/0266-5611/19/6/R01.

Weglein, A. B., F. A. Gasparotto, P. M. Carvalho, and R. H. Stolt, 1997, An inverse-scattering series method for attenuating multiples in seismic reflection data: Geophysics, **62**, 1975–1989, doi: 10.1190/1.1444298.

Yilmaz, Ö, 2001, Seismic data analysis: SEG.

Ziolkowski, A., D. B. Taylor, and R. G. K. Johnston, 1999, Marine seismic wavefield measurement to remove sea-surface multiples: Geophysical Prospecting, **47**, 841–870, doi: 10.1046/j.1365-2478.1999.00165.x.